In vivo assessment of shear modulus along the fibers of pennate muscle during passive lengthening and contraction using steered ultrasound push beams

Ricardo Andrade, Ha-Hien-Phuong Ngo, Alice Lemoine, Apolline Racapé, Nicolas Etaix, Thomas Frappart, Christophe Fraschini, Jean-Luc Gennisson, Antoine Nordez

journal of the mechanical behavior of biomedical materials 163 (2025) 106862

Contents lists available at ScienceDirect

Journal of the Mechanical Behavior of Biomedical Materials

journal homepage: www.elsevier.com/locate/jmbbm

In vivo assessment of shear modulus along the fibers of pennate muscle during passive lengthening and contraction using steered ultrasound push beams

Ricardo J. Andrade [a,**], Ha-Hien-Phuong Ngo [b], Alice Lemoine [c], Apolline Racapé [a], Nicolas Etaix [c], Thomas Frappart [c], Christophe Fraschini [c], Jean-Luc Gennisson [b,1], Antoine Nordez [a,d,1,*]

[a] Nantes Université, Mouvement - Interactions - Performance, MIP, UR 4334, F-44000, Nantes, France
[b] Laboratoire d'imagerie biomédicale multimodale (BioMaps), University Paris-Saclay, CEA, CNRS UMR 9011, Inserm UMR 1281, Orsay, F-91401, France
[c] Supersonic Imagine, Aix-en-Provence, France
[d] Institut Universitaire de France (IUF), Paris, France

ARTICLE INFO

Keywords:
Elastography
Tissue elasticity imaging
Medical imaging
Ultrasonography
Muscle

ABSTRACT

Ultrasound shear wave elastography (SWE) has emerged as a promising non-invasive method for muscle evaluation by assessing the propagation velocity of an induced shear wavefront. In skeletal muscles, the propagation of shear waves is complex, depending not only on the mechanical and acoustic properties of the tissue but also upon its geometry. This study aimed to comprehensively investigate the influence of muscle pennation angle on the shear wave propagation, which is directly related to the shear modulus. A novel elastography method based on steered pushing beams (SPB) was used to assess the shear modulus along the fibers of the *gastrocnemius medialis* (pennate) muscle in twenty healthy volunteers. Ultrasound scans were performed during passive muscle lengthening (n = 10) and submaximal isometric contractions (n = 10). The shear modulus along the fibers was compared to the apparent shear modulus, as commonly assessed along the muscle shortening direction using conventional SWE sequences. The shear modulus along the muscle fibers was significantly greater than the apparent shear modulus for passive dorsiflexion angles, while not significantly different throughout the range of plantar flexion angles (i.e., under any or very low tensile loads). The concomitant decrease in pennation angle along with the gradual increase in the shear modulus difference between the two methods as the muscle lengthens, strongly indicates that non-linear elasticity exerts a greater influence on wave propagation than muscle geometry. In addition, significant differences between methods were found across all submaximal contractions, with both shear modulus along the fibers and the pennation angle increasing with the contraction intensity. Specifically, incremental contraction intensity led to a greater bias than passive lengthening, which could be partly explained by distinct changes in pennation angle. Overall, the new SPB sequence provides a rapid and integrated geometrical correction of shear modulus quantification in pennate muscles, thereby eliminating the necessity for specialized systems to align the ultrasound transducer array with the fiber's orientation. We believe that this will contribute for improving the accuracy of SWE in biomechanical and clinical settings.

1. Introduction

Over the last two decades, ultrasound shear wave elastography (SWE) has emerged as a promising imaging technique, offering non-invasive tissue biomarkers with wide-ranging clinical applications (Barr et al., 2015; Cipriano et al., 2022) and enhancing our understanding of skeletal muscle function *in vivo* (Hug et al., 2015). Specifically, SWE provides real-time quantification of localized tissue shear modulus (an indicator of stiffness) by measuring the velocity of a remotely induced shear wavefront along the ultrasound probe direction

* Corresponding author. Nantes Université, Movement - Interactions - Performance, MIP, UR 4334, F-44000, Nantes, France.
** Corresponding author. Nantes Université, Movement - Interactions - Performance, MIP, UR 4334, F-44000, Nantes, France.
E-mail addresses: ricardo.andrade@univ-nantes.fr (R.J. Andrade), antoine.nordez@univ-nantes.fr (A. Nordez).
[1] Contributed equally.

https://doi.org/10.1016/j.jmbbm.2024.106862
Received 6 June 2024; Received in revised form 9 October 2024; Accepted 7 December 2024
Available online 8 December 2024

(Gennisson et al., 2013).

In the vast majority of human muscles, the fibers are angled relative to the muscle's axis of force generation (Lieber, 2022). This angle, also known as the pennation angle, makes it technically impossible to align the ultrasound transducer with the direction of the fibers. As a result, the assessment of the shear modulus using conventional SWE cannot be performed within the fiber's direction for pennate muscles. For this reason, it has been recommended to conduct SWE measurements along the muscle's shortening direction (Hug et al., 2015). This provides a measure of the "apparent" shear modulus (μ_{SWE}), within the physiological direction of the muscle – similar to how stiffness is assessed in tensile and contractile tests in animals. Interestingly, the shear wave propagation is influenced by both the transducer-fiber angle orientation (Gennisson et al., 2010) and the tensile state (Hug et al., 2015) such as that imposed by muscle lengthening or contractions (Hug et al., 2015). Therefore, because the pennation angle is also affected by the muscle tensile state (Fukunaga et al., 1997; Maganaris et al., 1998), predicting changes in shear modulus along the fiber direction with the measurements performed along the muscle's shortening direction is challenging and can lead to biased outcomes.

To our knowledge, only few a studies investigated the interplay between the pennation angle and the tensile state at different muscle lengths (Chino and Takahashi, 2018; Miyamoto et al., 2015) and during isometric contractions (Zimmer et al., 2023). They have used rotational approaches, which involve to manually or automatically rotate the transducer using gel pads or gel reservoirs placed on the skin to mimic a fusiform muscle. During passive lengthening at relatively small intensities, a significant bias between the shear modulus along the fibers and the apparent shear modulus has been observed (Chino and Takahashi, 2018; Miyamoto et al., 2015), albeit of minimal magnitude (i.e., <1.3%). On the contrary, Zimmer et al. (2023) showed a substantial bias at high isometric contraction levels. The differences between passive lengthening and contraction are likely to be explained by variations in the pennation angle, which decreases throughout a passive muscle lengthening (Fukunaga et al., 1997) and increases with higher levels of isometric contraction (Maganaris et al., 1998). Yet, it remains unclear whether differences in shear modulus estimates are mostly explained by changes in pennation angle or increased muscle loads. In addition, the differences in the rotational techniques used in previous studies raise serious questions about the ability to compare these studies.

A novel elastography method based on steered ultrasound push beams (SPB) has been recently developed to generate shear waves with a controlled propagation angle within the plane of the transducer array (Ngo et al., 2024a). This method enables the quantification of the shear modulus along the muscle fibers ($\mu_{\parallel SPB}$), regardless of the muscle pennation angle and without the need for time-consuming or specialized rotational approaches. In addition, it offers an elegant approach for better explore the differences between the apparent shear modulus μ_{SWE} and the shear modulus along the muscle fibers $\mu_{\parallel SPB}$.

The aim of the present study was to assess the $\mu_{\parallel SPB}$ of the pennate *gastrocnemius medialis* muscle during passive stretching and at different isometric contraction intensities to comprehensively investigate the interplay between muscle geometry (pennation angle) and elastography-measured passive and active muscle forces (shear modulus). We compared the shear modulus along the fibers $\mu_{\parallel SPB}$ with the apparent shear modulus μ_{SWE} assessed via conventional SWE sequences, as commonly used in numerous clinical and biomechanical studies. We hypothesized that $\mu_{\parallel SPB}$ would be greater than μ_{SWE}, and that this difference would increase with muscle lengthening and contraction levels, albeit to varying extends due to the opposing changes in pennation angle.

2. Methods

2.1. Participants

Two experiments were conducted to study the effects of pennation angle on shear modulus during passive muscle lengthening (Experiment I) and isometric contractions (Experiment II). A total of twenty healthy participants were enrolled in this study and underwent SWE scans: 10 participants (3 women; age: 20.8 ± 1.8 years; body mass 70.1 ± 10.1 kg; height: 174.7 ± 8.9) in Experiment I, and 10 participants (3 women; age: 22.3 ± 4.4 years; body mass 66.5 ± 9.7 kg; height: 175.3 ± 6.5) in Experiment II. The study was approved by the local institutional human research ethics committee (University of Nantes Human Research and Ethics Committee, CERNI n°IRB: IORG0011023) and all participants provided their written consent prior to testing.

2.2. Ultrasound shear wave elastography

For both experiments, SWE data were acquired using an ultrasound ultrafast device (Mach30, Hologic Supersonic Imagine, Aix-en-Provence, France) coupled with a linear transducer array (SL18-5, central frequency 7.5 MHz, 256 elements). The ultrasound transducer was aligned with *gastrocnemius medialis* muscle shortening direction. All ultrasound measurements were performed at 50% of muscle proximo-distal length, defined as the mid-distance between myotendinous junctions previously identified using B-mode. The center of the transducer array was aligned with the mid-muscle landmark. It was passively secured with a custom-made transducer holder to minimize the tissue pressure and movement-induced artifacts during scans.

A transversely isotropic material such as muscle tissue supports two modes of shear wave propagation: the shear horizontally polarized (SH; Equation 1) and shear vertical polarized (SV; Equation 2) modes, which are always polarized perpendicularly to each other and propagate with the following velocities (V):

- $\rho V_{SH}^2 = \mu_{\parallel}\, cos^2\,\theta + \mu_{\perp}\, sin^2\,\theta$ **(Equation 1, SH mode)**
- $\rho V_{SV}^2 = \mu_{\parallel} + (X_E \bullet \mu_{\perp} - \mu_{\parallel}) sin^2(2\theta),\ \text{with}\ X_E = \frac{E_{\parallel}}{E_{\perp}}$ **(Equation 2, SV mode)**

where ρ is the density assumed to be constant (approximately 1100 kg m^{-3}); $\mu_{\parallel}$ and $\mu_{\perp}$ are the shear modulus along and across the muscle fibers respectively; and X_E is the tensile anisotropy corresponding to the ratio of the Young's moduli parallel ($E_{\parallel}$) and perpendicular ($E_{\perp}$) to the muscle fibers and θ is the angle formed by the polarization vector (or push beam angle φ) and the transducer-to-fiber orientation (α). Conventional SWE sequences are designed to preferentially track the shear wave velocity of the SH propagation mode (V_{SH}^2) along the transducer's main axis. Specifically, the wave polarization vector is perpendicular to the plane formed by the material symmetry axis and wave propagation direction. The faster SV mode, defined by a wave polarization vector parallel to the plane formed by the material symmetry axis and wave propagation direction, can be detected in transverse isotropic materials by tilting the push beam with respect to the material's symmetry axis. The SV propagation mode (V_{SV}^2) can be modelled using the SPB sequence, which preferentially tracks the SV waves within the imaging plane of tilted configurations (e.g., pennate muscle geometry), to provide the shear modulus along the muscle fibers ($\mu_{\parallel SPB}$) (Ngo et al., 2024a).

Two different ultrasound sequences were used to quantify the shear modulus of the *gastrocnemius medialis*, characterized by a pennate muscle geometry. First, a conventional SWE sequence (Bercoff et al., 2004) was employed to quantify the muscle apparent shear modulus (μ_{SWE}) using the following relationship: $\mu = \rho V^2$. This sequence has been widely used to characterize muscle mechanical properties in research (Hug et al., 2015) and clinical (Cipriano et al., 2022) settings. Then, a

novel SPB sequence was used (Ngo et al., 2024a), enabling the quantification of shear modulus along the fibers ($\mu_{\|SPB}$) predicted by the SV propagation mode as described by Equation 2. Briefly, the SPB sequence was implemented in the ultrafast ultrasound scanner and modelled to capture the propagation of the SV wavefront. The push beams and the beamforming that enable the reconstruction of the propagation films were oriented with an angle φ ranging from $-18°$ to $18°$ with a gradual $2°$ increment (Fig. 1A). The push beams were electronically created by small apertures applying a delay law of an angle φ. The tracking ultrafast ultrasound sequence consisted of five tilted plane waves, oriented with the push beam angle φ (from $\varphi = -4°$ to $\varphi = +4°$, by $2°$ increments; Fig. 1B) (Montaldo et al., 2009). For each angle φ, four push lines were generated along the longitudinal axis of the ultrasound probe (Fig. 1C). For the 19 pushing angles φ, the total acquisition duration was approximately 6 s.

2.3. Experimental protocol

For both experiments, participants were seated in an isokinetic dynamometer (Biodex System 3 Pro, Biodex Medical, Shirley, NY) chair with the hips flexed at $125°$ ($180°$ = full extension) and the right knee fully extended. The chest and the waist were strapped to minimize trunk motion during acquisitions. The neutral position ($0°$) of the ankle was defined as an angle of $90°$ between the footplate and the shank. The lateral malleolus was used to estimate the center of rotation of the ankle and was aligned with the axis of the dynamometer. The foot was firmly strapped to avoid a potential heel displacement during the ankle rotations (Fig. 2A).

For the experiment I (muscle passive lengthening), shear wave elastography measurements were performed from $40°$ plantar flexion ($-40°$) to $20°$ dorsiflexion ($+20°$), with $5°$ increments (Fig. 2B). The sequence was immediately launched once the foot reached the targeted ankle angle, allowing to simultaneously acquire SWE and SPB data. To mitigate the impact of viscoelastic stress relaxation on SWE/SPB measurements (Freitas et al., 2015), the foot was promptly returned to the initial plantar flexion angle after each elastography acquisition. Then, the ankle was passively rotated ($2°$/s) into the next measurement angle for the subsequent elastography scan. This procedure was repeated until $20°$ of dorsiflexion. Surface electromyography (EMG) was recorded at 1 kHz (Biopac Systems Inc., Goleta, CA, USA) on gastrocnemius medialis and tibialis anterior muscles to ensure that muscles were passive during elastography acquisitions and ankle rotation (Le Sant et al., 2019). Two maximal voluntary isometric contractions in plantar flexion and dorsiflexion were performed to normalize the EMG values. The root mean square (RMS) of the EMG signals (RMS-EMG) was calculated every second over a 300-ms moving window for each ultrasound scan and normalized to the maximal voluntary isometric muscle activation test. All muscles were passive throughout all elastography measurements. Specifically, RMS-EMG was inferior to 1.5% for all scans regardless the ankle angle and, thus, may not have played a role in the elastography estimates during passive axial lengthening (Le Sant et al., 2019).

In the experiment II (contraction), shear modulus assessments were performed at different levels of isometric contraction of the gastrocnemius medialis. Following a standardized warm-up, participants were asked to perform two maximal voluntary isometric contractions (MVIC) in plantar flexion with the ankle joint in a neutral position ($90°$) for 3 s with 1 min rest interval in between. Ankle torque and EMG of the gastrocnemius medialis were simultaneously recorded at 1 kHz. The EMG-RMS was calculated in real time using a 300 ms moving average window. The maximum myoelectric activation across trials was considered as the best performance and then used to set the target level during the submaximal contractions. After 2 min of rest, visual EMG-RMS feedback was provided to the participants. They were carefully instructed to maintain a plateau for approximately 10 s at 5%, 10%, 15% and 20% of maximal EMG-RMS registered during the MVIC with a 1 min rest interval in between (Fig. 2C). The order of the contractions was randomized. For all contraction levels, elastography scans were performed at the plateau. An additional measurement was performed at a resting state. For both experiments, joint angle, ankle torque and EMG data were acquired using a Biopac system (Biopac Systems Inc., Goleta, CA, USA).

2.4. Data processing

All ultrasound-based data (SWE/SPB) was processed offline in Matlab® (2022a, Mathworks, Natick, MA, USA) using custom scripts. For the conventional SWE sequence, the entire procedure was performed in accordance with the framework of the commercial sequence of ultrafast scanner (Bercoff et al., 2004), leading to a direct estimate of the apparent shear modulus (μ_{SWE}) using equation 1 (V_{SH}^2). For the SPB

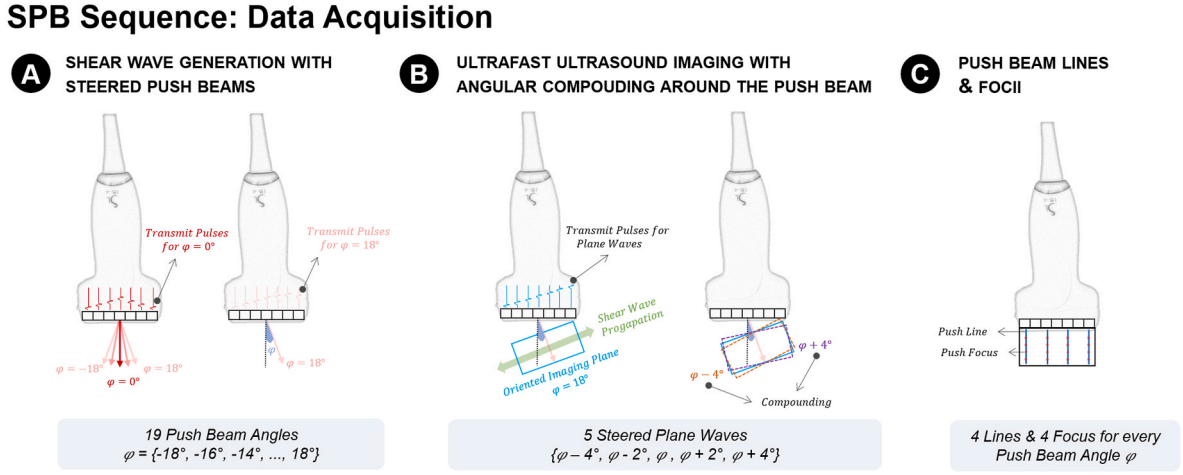

Fig. 1. Steered Push Beam (SPB) sequence used to generate and track the shear vertical (SV) propagation mode. (A) The ultrasound transducer array was positioned parallel to the muscle's shortening direction of a pennate muscle and remains stationary for all measurements. Nineteen steered push beams were electronically programmed with an angle φ (from $-18°$ to $18°$, with a $2°$ increment) to generate different focused acoustic radiation forces that create shear waves with a given propagation vector. Please note that conventional ultrasound elastography sequences use a single push beam angle ($\varphi = 0°$) to create the shear wave front. (B) Ultrafast ultrasound plane waves were used to track the propagating shear wave fronts. For each push beam φ, 5 steered plane waves (from $-4°$ to $4°$, with a $2°$ increment) were used to track the respective propagating shear wave fronts. (C) Each push beam with an angle φ, was repeated 4 times at different locations along the main direction of the transducer (push lines). Four push focus were programmed along each push line.

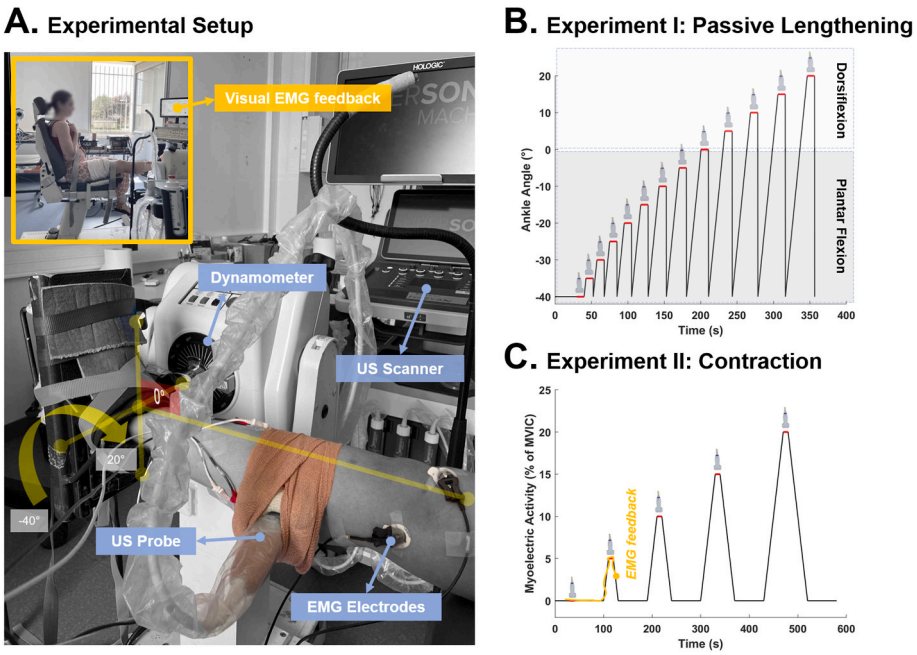

Fig. 2. Experimental setup. (A) For both experiments, participants were seated in an isokinetic dynamometer (Biodex System 3 Pro, Biodex Medical, Shirley, NY) with the right knee fully extended. All ultrasound measurements were performed at the *gastrocnemius medialis* muscle, at the mid-distance between proximal and distal myotendinous junctions previously identified using B-mode. Ultrasound data and EMG signals were simultaneously recorded from the *gastrocnemius medialis* muscle during passive lengthening – from 40° plantar flexion (−40°) and 20° dorsiflexion (B; Experiment I) – and while participants performed isometric contractions with visual real-time EMG feedback (C; Experiment II).

sequence, the fiber's angle in respect to the transducer's face α was initially measured on a previously recorded B-mode image for each ankle angle (Fig. 3A). This angle was used to perform a beamforming with specular reconstruction. The shear wave velocity was then tracked by applying a time-of-flight algorithm (Deffieux et al., 2012; Loupas et al., 1995) to the recorded shear wave propagation films (Bercoff et al., 2004) (Fig. 3B). A directional filter was further applied. Finally, the recombination across the four push lines was performed to create a shear wave map for the different aperture angles (Fig. 3C). Finally, the shear modulus along the muscle fibers ($\mu_{\|SPB}$) was quantified by fitting the group shear wave velocity data (one value per aperture angle φ) with equation 2, which governs the SV propagation mode (V_{SV}^2) (Fig. 3D). The

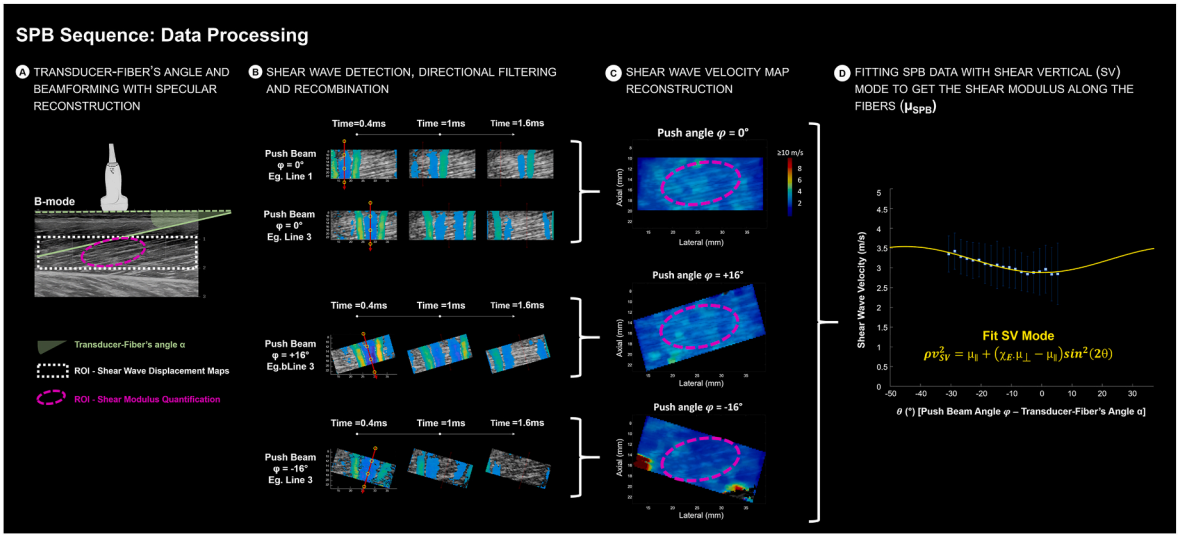

Fig. 3. Data processing steps for the data acquired with the SPB sequence. (A) Measurement of the fiber's angle α in respect to the transducer's face was initially measured for each ankle angle and contraction level, followed by a beamforming with specular reconstruction. **(B)** The shear wave velocity was tracked by applying a time-of-flight algorithm to the recorded shear wave propagation films. A directional filter was further applied, and a recombination was performed across the four push lines to create a shear wave map for the different aperture angles (i.e., steered push beams). Typical examples of the propagation films (frames at 0.4 ms, 1 ms and 1.6 ms) for push beam angles φ = 0°, φ = 16°, and φ = -16° are illustrated. For the push beam angle φ = 0°, two push lines (1 and 3) are depicted as typical example. **(C)** Shear wave velocity maps were then reconstructed for each push beam. An ellipsoidal ROI was drawn across the different reconstructed shear wave velocity maps to identify the same muscle region across the push beams. **(D)** The shear wave velocity within each ROI/push beam angle was averaged and the shear modulus along the muscle fibers ($\mu_{\|SPB}$) was calculated using Equation 2 for the SV propagation mode, as described in the graphic. The apparent shear modulus (μ_{SWE}) was quantified using the relationship $\mu = \rho V^2$ from the measurements at push beam angle = 0°.

same region of interest (ROI) was used to quantify the muscle shear modulus from both SWE and SPB propagation films across muscle lengthening incremental steps and contractions levels. In addition, for the SPB, the same ROI coordinates were used for each steered push beam (Fig. 3C). Specifically, an ellipsoidal ROI with a radius of approximately 4–5 mm was drawn, as illustrated in Fig. 3A and C, to measure the same exact muscle region across push aperture angles φ.

2.5. Statistical analysis

Statistical analyses were performed using one-dimensional statistical parametric mapping (SPM) allowing the analysis of continuous data, especially the muscle shear modulus as a function of ankle angle and contraction levels. A custom Matlab code (MathWorks, Inc., Natick, USA) was used to conduct SPM analyses implementing functions from the open source spm1d package (http://www.spm1d.org, version M.0.4.7) as described by Pataky (2012). Prior to any inferential procedure, data normality was assessed with the built-in function 'spm1d.stats.normality.sw' for the Shapiro-Wilk test. Using SPM, a two-tailed, paired *t*-test was conducted to compare the gastrocnemius medialis shear modulus measured by each elastography method ($\mu_{\|SPB}$ *versus* μ_{SWE}) across all the ankle angles and contraction levels. The significance level for all statistical comparisons was set to $p < 0.05$.

In addition, a comparison of the difference in shear modulus deviation between both elastography sequences, SPB and SWE, was performed using the Bland-Altman method for analysis of measurement agreement. Both methods were compared across four ankle angles (i.e., −40°, 20°, 0° and 20°) corresponding to different muscle axial loading states. Similarly, comparisons at different contraction levels (0%, 5%, 10%, 15% and 20% of maximal EMG-RMS) were conducted. Graphics were performed in GraphPad Prism (version 9.0; GraphPad Software, Inc., CA, US). Descriptive data are presented as mean ± standard deviation.

3. Results

3.1. Muscle passive lengthening (experiment I)

For all ankle angles the mean $\mu_{\|SPB}$ was consistently higher than the mean μ_{SWE}. However, significant differences in shear modulus were only observed in dorsiflexed angles where muscle is under axial tensile load (all $p < 0.01$; Fig. 4A). The Bland-Altman plots illustrate a systematic bias ranging from 0.3 to 4.1 kPa between the methods across four different axial tensile loads (ankle angles: 40° and 20° plantar flexion; neutral position 0°; and 20° dorsiflexion). An increase in bias was observed towards dorsiflexed angles (Fig. 5), where the muscle shear modulus increases and the pennation angle decreases as the muscle lengthens (Fig. 4B).

3.2. Muscle contraction (experiment II)

Averaged myoelectric activity of the *gastrocnemius medialis* during the elastography acquisitions for 0%, 5%, 10%, 15% and 20% was 0.4% ± 0.4%, 6.0% ± 1.4%, 9.9% ± 1.4%, 15.0% ± 1.7% and 19.5% ± 1.7% respectively. For all contraction levels, $\mu_{\|SPB}$ was significantly higher than μ_{SWE} (all $p < 0.01$; Fig. 4C). The magnitude of the differences increased with the increase in the contraction level, which was associated with an increase in pennation angle (Fig. 4D).

Bland and Altman analyses illustrate a systematic bias between methods, ranging from 4.3 to 19 kPa across the four different contraction intensities (Fig. 6). Bias increased with the progressive increase in the gastrocnemius myoeletric activity (from 0 to 20% of MVIC), which is associated with higher active muscle tension and increased pennation angle increase. This indicates that conventional SWE method underestimates the shear modulus compared to the novel SPB during isometric contractions.

4. Discussion

In this study we provide a comprehensive insight into the complex

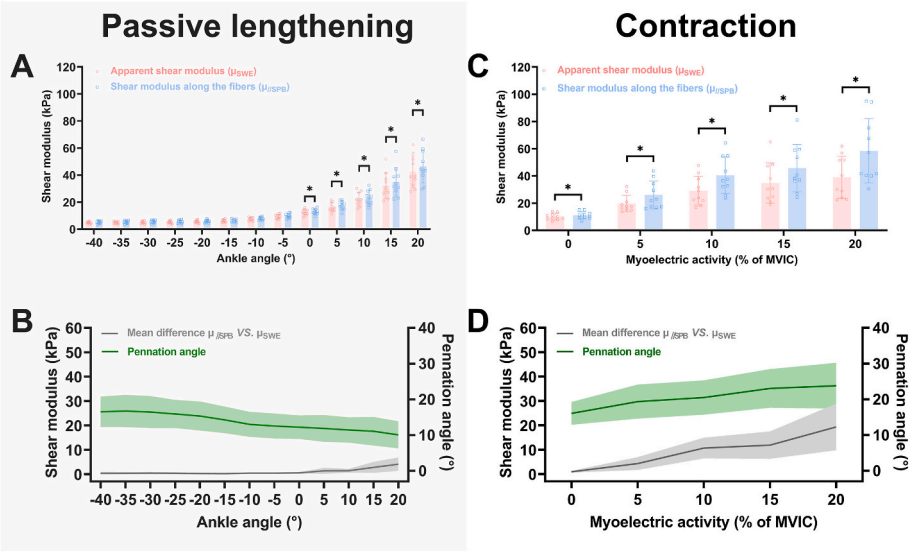

Fig. 4. *Gastrocnemius medialis* shear modulus along the fibers measured by SPB method, and the apparent shear modulus, as assessed by conventional SWE. **(A)** Averaged shear modulus quantified by SPB (blue) and SWE (red) methods during a passive ankle rotation. Negative ankle angles correspond to plantar flexion angles (*gastrocnemius medialis* shortened) and positive ankle angles correspond to dorsiflexion angles (*gastrocnemius medialis* under passive tensile loading). Circle (◯) and square (□) symbols denote individual data. **(B)** Averaged difference in shear modulus between both methods (gray) and pennation angle (green) throughout muscle lengthening. **(C)** Averaged shear modulus quantified by SPB (blue) and SWE (red) methods for different levels of submaximal isometric contractions, expressed as percentage of myoelectric activation (EMG-RMS). Circle (◯) and square (□) symbols denote individual data. **(D)** Averaged difference in shear modulus between both methods (gray) and pennation angle (green) as a function of contraction intensity. *p value < 0.05. (For interpretation of the references to colour in this figure legend, the reader is referred to the Web version of this article.)

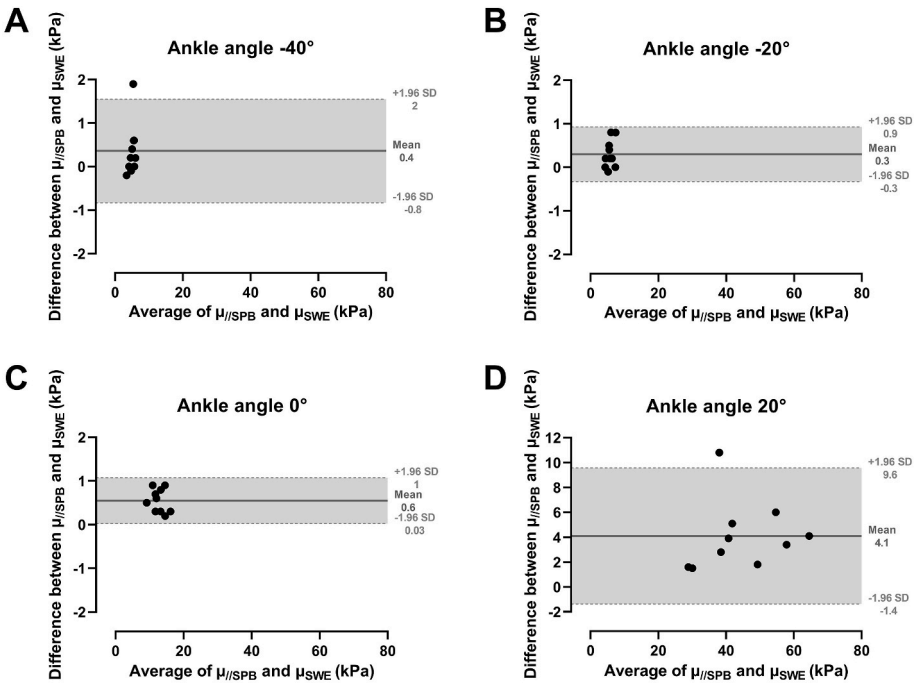

Fig. 5. Bland-Altman plots comparing the *gastrocnemius medialis* shear modulus assessed by the SPB sequence (shear modulus along the muscle fibers) and by conventional shear wave elastography (apparent shear modulus) for 4 different ankle angles. Graphic titles with negative ankle angles correspond to plantar flexion angles (*gastrocnemius medialis* shortened) and positive ankle angles correspond to dorsiflexion angles (*gastrocnemius medialis* under passive tensile loading). Bias (solid gray lines) and upper and lower limits of agreement (dashed gray lines) with corresponding values are displayed. $\mu_{\|SPB}$: shear modulus along the muscle fibers; μ_{SWE}: apparent shear modulus.

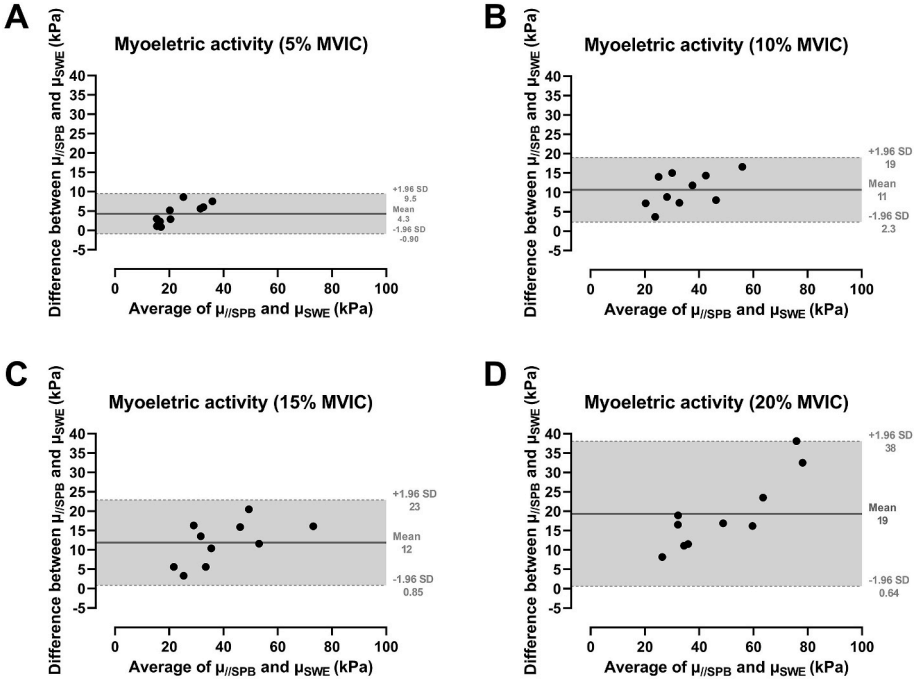

Fig. 6. Bland-Altman plots comparing the gastrocnemius medialis shear modulus assessed by the SPB sequence (shear modulus along the muscle fibers) and by conventional shear wave elastography (apparent shear modulus) for 4 different submaximal contraction intensities based on myoelectric intensity. Bias (solid gray lines) and upper and lower limits of agreement (dashed gray lines) with corresponding values are displayed. MVIC: muscle voluntary isometric contraction; $\mu_{\|SPB}$: shear modulus along the muscle fibers; μ_{SWE}: apparent shear modulus.

interplay between muscle geometry (pennation angle), muscle (active and passive) loading and the shear wave propagation. We quantified the differences between the apparent shear modulus μ_{SWE}, as commonly assessed by conventional SWE sequences, and the shear modulus along the muscle fibers $\mu_{\|SPB}$ quantified by a novel SPB method during muscle contraction and passive lengthening, known to modify pennation angle. In accordance with our hypothesis, the findings of the present study demonstrate a consistent underestimation bias in shear modulus quan-

tification when using a conventional SWE sequence compared to the shear modulus along the muscle fibers. While this underestimation was not significant at resting states without any active and passive tension, it increased considerably at higher muscle tensile loads involving both passive and active muscle tension. In addition, we also found that shear wave propagation is affected by muscle geometry to a greater extent during isometric contractions, characterized by an increase in pennation angle with increasing load, compared to passive lengthening, during which the pennation angle decreases with increasing axial tensile load. These results demonstrate the importance in considering not only the transducer-muscle fiber alignment (i.e., anisotropy), but also the nonlinear mechanics when modeling shear forces in physiologically loaded muscle tissue.

The shear modulus values obtained for the *gastrocnemius medialis* at each ankle angle during the passive stretching (Experiment I) and the shape of shear modulus-ankle angle relationships align with those reported in previous studies involving healthy individuals (e.g., Andrade et al., 2020, 2018; Le Sant et al., 2017; Maisetti et al., 2012). The non-significant differences observed between SPB and SWE methods at shortening lengths (plantar flexion angles) are consistent with recent observations, where probe-muscle alignment approaches were used to artificially modify the muscle pennation angle within the imaging plane. The same absolute differences were reported by a previous study for SWE evaluations performed at 30°, 20°, 10° of ankle plantar flexion (Chino and Takahashi, 2018). Such magnitude of differences (~0.6 kPa) agrees with those observed in the present study within the plantar flexion range (Fig. 2B). Overall, these observations demonstrate that fiber's orientation relative to the transducer array has only minimal influence on shear modulus quantification for muscles under low passive loads, thereby limiting the potential added value of the SPB sequences used in such conditions. However, a novel finding was that this bias increased towards greater passive axial muscle loads (dorsiflexion angles). Specifically, the concomitant decrease in muscle pennation angle observed throughout the muscle axial passive lengthening was accompanied by an increase in the difference between the longitudinal and the apparent shear moduli (Fig. 2B). This finding is not in accordance with Miyamoto et al. (2015), who observed a marginal effect of the probe rotation of 20° within the imaging plane compared to no alignment, assessed at 0°, 10° and 20° of ankle dorsiflexion (<1.3%, corresponding to an absolute difference of 0.6 ± 0.5 kPa). Furthermore, this previous study did not observe any interaction between transducer angle and ankle angle, which is not consistent with our results. These differences across both studies may be explained by the differences in the method used to quantify the shear modulus. We believe that the SPB method is more sensible and accurate than the transducer alignment method used by Miyamoto et al. (2015). Furthermore, the finding demonstrating a progressive increase in the difference between the apparent shear modulus and the shear modulus along the fibers during passive lengthening, strongly suggest that non-linear elasticity (Bied and Gennisson, 2021; Ngo et al., 2024b) exerts a greater influence on wave propagation than the muscle geometry. Further works are required to better understand the influence of nonlinear elasticity on the shear wave propagation in anisotropic tissues such as muscles.

For the isometric contractions (Experiment II), the shear modulus along the fibers was consistently higher than apparent shear modulus. This was observed from rest (ankle neutral position = 0°) to 20% of maximal voluntary isometric contraction, as measured by local myoelectric activity. However, the bias increased considerably towards greater contraction intensities. This finding aligns with a recent *in vivo* study (Zimmer et al., 2023) that observed significant differences between probe alignment (manual or automatic system) *versus* no alignment for the same pennate muscle, which amplify with increased muscle activity. Specifically, greater shear wave velocities were found during aligned conditions, being the differences against no alignment more pronounced at higher isometric contraction intensities (i.e., >50% of maximal isometric voluntary contraction expressed as % of ankle torque), where the fiber's angle also increase considerably (>20°). However, our method showed greater differences for 20% of myoelectric activity of MVIC (approximatively 34.8% ± 6.75% of MVIC based on of peak torque measurements) than those reported by Zimmer et al. at 50%, 75% and MVIC. Globally, these differences may be mainly driven by the increased pennation angle with increased level of the isometric contraction. Furthermore, incremental contraction intensity led to a greater bias than that observed during passive lengthening, which could be partly explained by distinct changes in pennation angle. However, the concomitant decrease in pennation angle and gradual increase in the difference between the two methods during the muscle lengthening strongly indicates that non-linear elasticity exerts a greater influence on wave propagation than muscle geometry, especially under significant tensile axial loads.

The SPB technique provides a novel method that eliminates the need for manual or automatic adjustment of the ultrasound probe to mimic a fusiform muscle geometry. Measuring the shear modulus along muscle fibers may enhance the accuracy of clinical evaluation using ultrasound elastography, especially in neuromuscular conditions such as Duchenne and Becker's muscular dystrophies, where muscle structural and geometrical properties are altered (Briguet et al., 2004; Hooijmans et al., 2015). The SPB technique also enables the study of muscle anisotropy (Ngo et al., 2024a) and, when combined with other methods, non-linear elasticity (Ngo et al., 2024b), offering potentially valuable clinical perspectives. Additionally, it may contribute to improving the accuracy of longitudinal measurements of muscle shear modulus in cases where muscle geometry and the mechanical properties are concomitantly modified (e.g., responses to exercise training such as resistance and stretching training, and neuromuscular disorders).

In this study the SPB method was exclusively used to assess the mechanical properties of the *gastrocnemius medialis*. This muscle has been widely studied using 2D ultrasound due to its 2D organization and the ability to identify a consistent and unique 2D plane for the fascicles, regardless of the contraction or lengthening levels (Lichtwark et al., 2007). However, SPB may present more challenges for studying muscles exhibiting a more complex architecture such triangular/convergent (e.g., gluteus maximus, pectoralis major) and circular. The development of 3D ultrasound with matrix phased arrays (Gennisson et al., 2015) would provide a 3D analysis of muscle anisotropy, which could be highly relevant for such complex musculature. To this end, the 2D SPB technique used in the present study will have to be developed in 3D.

5. Conclusion

The quantification of the apparent shear modulus μ_{SWE} in skeletal muscles using conventional SWE sequences is influenced by the fiber's direction. Here, we comprehensively quantified the influence of the pennation angle on the shear wave propagation and the estimates of the shear modulus. Overall, conventional SWE underestimated the muscle shear modulus assessed in the pennate muscle geometry of the *gastrocnemius medialis* compared to that obtain via the SPB sequence. However, this underestimation was marginal and non-significant for the low muscle passive tensile loads. Moreover, the concomitant decrease in muscle pennation angle observed throughout the passive muscle lengthening was accompanied by an increase in the difference between the shear modulus along the fibers and the apparent shear moduli. These observations strongly suggest that anisotropic nonlinear shear elasticity may have a more significant impact on the quantification of the muscle shear modulus than muscle geometry under considerable tensile (active and passive) loads. Further studies are required to better understand muscle anisotropy with the SPB method and consider the ability of such technique to provide novel biomarkers that may be useful to assess muscle tissue in various clinical situations.

CRediT authorship contribution statement

Ricardo J. Andrade: Writing – review & editing, Writing – original draft, Visualization, Software, Methodology, Investigation, Formal analysis, Data curation, Conceptualization. **Ha-Hien-Phuong Ngo:** Writing – review & editing, Software, Methodology. **Alice Lemoine:** Writing – review & editing, Software, Methodology. **Apolline Racapé:** Writing – review & editing, Investigation, Formal analysis, Data curation. **Nicolas Etaix:** Writing – review & editing, Software, Resources, Methodology. **Thomas Frappart:** Writing – review & editing, Software, Resources, Methodology. **Christophe Fraschini:** Writing – review & editing, Software, Resources, Methodology. **Jean-Luc Gennisson:** Writing – review & editing, Writing – original draft, Software, Resources, Project administration, Methodology, Investigation, Funding acquisition, Conceptualization. **Antoine Nordez:** Writing – review & editing, Writing – original draft, Resources, Project administration, Methodology, Investigation, Funding acquisition, Conceptualization.

Availability of data

The datasets used are available from the corresponding author on reasonable request.

Declaration of competing interest

The authors declare that they have no known competing financial interests or personal relationships that could have appeared to influence the work reported in this paper.

Acknowledgements

This work was funded by ANR INNOVAN (ANR-19-CE19-0017) and supported by AFM-Téléthon (Grant ID#28643 to Ricardo J. Andrade). We thank Mar Hernández-Secorún and Macéo Renault for their help with data collection.

Data availability

Data will be made available on request.

References

Andrade, R.J., Freitas, S.R., Hug, F., Le Sant, G., Lacourpaille, L., Gross, R., McNair, P., Nordez, A., 2018. The potential role of sciatic nerve stiffness in the limitation of maximal ankle range of motion. Sci. Rep. 8, 14532. https://doi.org/10.1038/s41598-018-32873-6.

Andrade, R.J., Freitas, S.R., Hug, F., Le Sant, G., Lacourpaille, L., Gross, R., Quillard, J.B., McNair, P.J., Nordez, A., 2020. Chronic effects of muscle and nerve-directed stretching on tissue mechanics. J. Appl. Physiol. 129, 1011–1023. https://doi.org/10.1152/japplphysiol.00239.2019, 1985.

Barr, R.G., Ferraioli, G., Palmeri, M.L., Goodman, Z.D., Garcia-Tsao, G., Rubin, J., Garra, B., Myers, R.P., Wilson, S.R., Rubens, D., Levine, D., 2015. Elastography assessment of liver fibrosis: society of radiologists in ultrasound consensus conference statement. Radiology 276, 845–861. https://doi.org/10.1148/radiol.2015150619.

Bercoff, J., Tanter, M., Fink, M., 2004. Supersonic shear imaging: a new technique for soft tissue elasticity mapping. Ieee Trans Ultrason Ferroelectr Freq Control 51, 396–409.

Bied, M., Gennisson, J.-L., 2021. Acoustoelasticity in transversely isotropic soft tissues: quantification of muscle nonlinear elasticity. J. Acoust. Soc. Am. 150, 4489–4500. https://doi.org/10.1121/10.0008976.

Briguet, A., Courdier-Fruh, I., Foster, M., Meier, T., Magyar, J.P., 2004. Histological parameters for the quantitative assessment of muscular dystrophy in the mdx-mouse. Neuromuscul. Disord. 14, 675–682. https://doi.org/10.1016/j.nmd.2004.06.008.

Chino, K., Takahashi, H., 2018. Influence of pennation angle on measurement of shear wave elastography: *in vivo* observation of shear wave propagation in human pennate muscle. Physiol. Meas. 39, 115003. https://doi.org/10.1088/1361-6579/aae7e2.

Cipriano, K.J., Wickstrom, J., Glicksman, M., Hirth, L., Farrell, M., Livinski, A.A., Esfahani, S.A., Maldonado, R.J., Astrow, J., Berrigan, W.A., Piergies, A.M.H., Hobson-Webb, L.D., Alter, K.E., 2022. A scoping review of methods used in musculoskeletal soft tissue and nerve shear wave elastography studies. Clin. Neurophysiol. 140, 181–195. https://doi.org/10.1016/j.clinph.2022.04.013.

Deffieux, T., Gennisson, J.-L., Larrat, B., Fink, M., Tanter, M., 2012. The variance of quantitative estimates in shear wave imaging: theory and experiments. IEEE Trans. Ultrason. Ferroelectr. Freq. Control 59, 6343266. https://doi.org/10.1109/TUFFC.2012.2472.

Freitas, S.R., Andrade, R.J., Larcoupaille, L., Mil-homens, P., Nordez, A., 2015. Muscle and joint responses during and after static stretching performed at different intensities. Eur. J. Appl. Physiol. 115, 1263–1272. https://doi.org/10.1007/s00421-015-3104-1.

Fukunaga, T., Ichinose, Y., Ito, M., Kawakami, Y., Fukashiro, S., 1997. Determination of fascicle length and pennation in a contracting human muscle in vivo. J. Appl. Physiol. 82, 354–358. https://doi.org/10.1152/jappl.1997.82.1.354.

Gennisson, J.L., Deffieux, T., Fink, M., Tanter, M., 2013. Ultrasound elastography: principles and techniques. Diagn Interv Imaging 94, 487–495. https://doi.org/10.1016/j.diii.2013.01.022.

Gennisson, J.L., Deffieux, T., Mace, E., Montaldo, G., Fink, M., Tanter, M., 2010. Viscoelastic and anisotropic mechanical properties of in vivo muscle tissue assessed by supersonic shear imaging. Ultrasound Med. Biol. 36, 789–801. https://doi.org/10.1016/j.ultrasmedbio.2010.02.013.

Gennisson, J.L., Provost, J., Deffieux, T., Papadacci, C., Imbault, M., Pernot, M., Tanter, M., 2015. 4-D ultrafast shear-wave imaging. Ieee Trans Ultrason Ferroelectr Freq Control 62, 1059–1065. https://doi.org/10.1109/TUFFC.2014.006936.

Hooijmans, M.T., Damon, B.M., Froeling, M., Versluis, M.J., Burakiewicz, J., Verschuuren, J.J.G.M., Niks, E.H., Webb, A.G., Kan, H.E., 2015. Evaluation of skeletal muscle DTI in patients with duchenne muscular dystrophy. NMR Biomed. 28, 1589–1597. https://doi.org/10.1002/nbm.3427.

Hug, F., Tucker, K., Gennisson, J.L., Tanter, M., Nordez, A., 2015. Elastography for muscle biomechanics: toward the estimation of individual muscle force. Exerc. Sport Sci. Rev. 43, 125–133. https://doi.org/10.1249/JES.0000000000000049.

Le Sant, G., Gross, R., Hug, F., Nordez, A., 2019. Influence of low muscle activation levels on the ankle torque and muscle shear modulus during plantar flexor stretching. J. Biomech. 93, 111–117. https://doi.org/10.1016/j.jbiomech.2019.06.018.

Le Sant, G., Nordez, A., Andrade, R., Hug, F., Freitas, S., Gross, R., 2017. Stiffness mapping of lower leg muscles during passive dorsiflexion. J. Anat. 230, 639–650. https://doi.org/10.1111/joa.12589.

Lichtwark, G.A., Bougoulias, K., Wilson, A.M., 2007. Muscle fascicle and series elastic element length changes along the length of the human gastrocnemius during walking and running. J. Biomech. 40, 157–164. https://doi.org/10.1016/j.jbiomech.2005.10.035.

Lieber, R.L., 2022. Can we just forget about pennation angle? J. Biomech. 132, 110954. https://doi.org/10.1016/j.jbiomech.2022.110954.

Loupas, T., Powers, J.T., Gill, R.W., 1995. An axial velocity estimator for ultrasound blood flow imaging, based on a full evaluation of the Doppler equation by means of a two-dimensional autocorrelation approach. IEEE Trans. Ultrason. Ferroelectr. Freq. Control 42, 672–688. https://doi.org/10.1109/58.393110.

Maganaris, C.N., Baltzopoulos, V., Sargeant, A.J., 1998. *In vivo* measurements of the triceps surae complex architecture in man: implications for muscle function. J. Physiol. 512, 603–614. https://doi.org/10.1111/j.1469-7793.1998.603be.x.

Maisetti, O., Hug, F., Bouillard, K., Nordez, A., 2012. Characterization of passive elastic properties of the human medial gastrocnemius muscle belly using supersonic shear imaging. J. Biomech. 45, 978–984. https://doi.org/10.1016/j.jbiomech.2012.01.009.

Miyamoto, N., Hirata, K., Kanehisa, H., Yoshitake, Y., 2015. Validity of measurement of shear modulus by ultrasound shear wave elastography in human pennate muscle. PLoS One 10, e0124311. https://doi.org/10.1371/journal.pone.0124311.

Montaldo, G., Tanter, M., Bercoff, J., Benech, N., Fink, M., 2009. Coherent plane-wave compounding for very high frame rate ultrasonography and transient elastography. IEEE Trans. Ultrason. Ferroelectr. Freq. Control 56, 489–506. https://doi.org/10.1109/TUFFC.2009.1067.

Ngo, H.-H.-P., Andrade, R.J., Brum, J., Benech, N., Chatelin, S., Loumeaud, A., Frappart, T., Fraschini, C., Nordez, A., Gennisson, J.-L., 2024a. In plane quantification of in vivo muscle elastic anisotropy factor by steered ultrasound pushing beams. Phys. Med. Biol. https://doi.org/10.1088/1361-6560/ad21a0.

Ngo, H.-H.-P., Andrade, R.J., Lancelot, J., Loumeaud, A., Cornu, C., Nordez, A., Chatelin, S., Gennisson, J.-L., 2024b. Unravelling anisotropic nonlinear shear elasticity in muscles: towards a non-invasive assessment of stress in living organisms. J. Mech. Behav. Biomed. Mater. 150, 106325. https://doi.org/10.1016/j.jmbbm.2023.106325.

Pataky, T.C., 2012. One-dimensional statistical parametric mapping in Python. Comput. Methods Biomech. Biomed. Engin. 15, 295–301. https://doi.org/10.1080/10255842.2010.527837.

Zimmer, M., Bunz, E.K., Ehring, T., Kaiser, B., Kienzlen, A., Schlüter, H., Zürn, M., 2023. In vivo assessment of shear wave propagation in pennate muscles using an automatic ultrasound probe alignment system. IEEE Open J. Eng. Med. Biol. 4, 259–267. https://doi.org/10.1109/OJEMB.2023.3338090.